Neurobiology of Disease

Mild Intraocular Pressure Elevation in Mice Reveals Distinct Retinal Ganglion Cell Functional Thresholds and Pressure-Dependent Properties

Xiaofeng Tao,[1] Jasdeep Sabharwal,[1,2] Robert L. Seilheimer,[1] Samuel M. Wu,[1,2] and Benjamin J. Frankfort[1,2]
[1]Department of Ophthalmology, and [2]Department of Neuroscience, Baylor College of Medicine, Houston, Texas 77030

Elevation of intraocular pressure (IOP) causes retinal ganglion cell (RGC) dysfunction and death and is a major risk factor for glaucoma. We used a bead injection technique to increase IOP in mice of both genders by an average of ~3 mmHg for 2 weeks. This level of IOP elevation was lower than that achieved in other studies, which allowed for the study of subtle IOP effects. We used multielectrode array recordings to determine the cellular responses of RGCs exposed to this mild degree of IOP elevation. We found that RGC photopic receptive field (RF) center size and whole-field RGC firing rates were unaffected by IOP elevation. In contrast, we found that the temporal properties of RGC photopic responses in the RF center were accelerated, particularly in ON sustained cells. We also detected a loss of antagonistic surround in several RGC subtypes. Finally, spontaneous firing rate, interspike interval variance, and contrast sensitivity were altered according to the magnitude of IOP exposure and also displayed an IOP-dependent effect. Together, these results suggest that individual RGC physiologic parameters have unique IOP-related functional thresholds that exist concurrently and change following IOP elevation according to specific patterns. Furthermore, even subtle IOP elevation can impart profound changes in RGC function, which in some cases may occur in an IOP-dependent manner. This system of overlapping functional thresholds likely underlies the complex effects of elevated IOP on the retina.

Key words: cellular function; glaucoma; intraocular pressure; IOP; retinal ganglion cell; RGC

Significance Statement

Retinal ganglion cells (RGCs) are the obligate output neurons of the retina and are injured by elevated intraocular pressure (IOP) in diseases such as glaucoma. In this study, a subtle elevation of IOP in mice for 2 weeks revealed distinct IOP-related functional thresholds for specific RGC physiologic parameters and sometimes showed an IOP-dependent effect. These data suggest that overlapping IOP-related thresholds and response profiles exist simultaneously in RGCs and throughout the retina. These overlapping thresholds likely explain the range of RGC responses that occur following IOP elevation and highlight the wide capacity of neurons to respond in a diseased state.

Introduction

Glaucoma is a chronic, progressive neurodegeneration of the optic nerve and is a major public health issue (Congdon et al., 2004; Quigley and Broman, 2006). The primary cells injured in glaucoma are retinal ganglion cells (RGCs) and RGC axon and soma injury are important components of the disease. Currently, all approved treatments for glaucoma are aimed at the reduction of intraocular pressure (IOP), which is the only modifiable risk factor (Heijl et al., 2002; Kass et al., 2002). Furthermore, clinical studies show that the amount of IOP reduction is important and patients have improved outcomes with increased IOP reduction (AGIS Investigators, 2000; Leske et al., 2003). Interestingly, glaucoma occurs at normal IOP in a large percentage of patients and those patients similarly benefit from the reduction of IOP (Collaborative Normal-Tension Glaucoma Study Group, 1998).

Despite this reliance on IOP reduction for treatment, there remain major gaps in our understanding of how IOP affects RGCs on a cellular level. A recent area of interest is the impact of increased IOP on RGC subtypes, of which at least 30 have been

Received Aug. 14, 2018; revised Dec. 18, 2018; accepted Jan. 3, 2019.

Author contributions: X.T. wrote the first draft of the paper; J.S., R.L.S., S.M.W., and B.J.F. edited the paper. X.T., J.S., and B.J.F. designed research; X.T. performed research; X.T., J.S., R.L.S., and B.J.F. analyzed data; X.T. and B.J.F. wrote the paper.

This work was supported by the National Institutes of Health (R01 Grant EY025601 to B.J.F., Grant EY019908 to S.M.W., and Grant EY004446 to S.M.W., Vision Core Grant EY002520, and a Visual Science Training Program Grant EY007001), the Retina Research Foundation (Houston, TX), and an unrestricted grant from Research to Prevent Blindness (New York, NY) to Baylor College of Medicine.

The authors declare no competing financial interests.

Correspondence should be addressed to Benjamin J. Frankfort at benjamin.frankfort@bcm.edu.

https://doi.org/10.1523/JNEUROSCI.2085-18.2019

 0270-6474/19/391881-11$15.00/0

identified physiologically and at least 40 have been identified by single-cell RNA sequencing (Baden et al., 2016; Rheaume et al., 2018). Multiple groups have now reported differences in the susceptibilities of specific RGC subtypes to IOP-induced injury on both the structural and functional level (Della Santina et al., 2013; Feng et al., 2013; El-Danaf and Huberman, 2015; Ou et al., 2016; Sabharwal et al., 2017; Risner et al., 2018). In addition, several lines of evidence suggest that upstream retinal circuitry and synapse fidelity are also affected by elevated IOP (Pang et al., 2015; Ou et al., 2016; Sabharwal et al., 2017). Therefore, glaucoma likely occurs as a complex relationship involving both differential phenotypes of RGC subtypes and abnormal interactions among multiple retinal cell types.

Within this environment, it is possible that the magnitude of IOP elevation is responsible for some aspects of these differential effects, but a relationship between IOP level and RGC functional changes in mice has not been clearly established (Della Santina et al., 2013; Frankfort et al., 2013). One potential explanation for this inconsistency is the wide range of IOP elevation models used and the relatively high IOP increases generated. Here, we address this knowledge gap by elevating IOP in mice using a version of the bead injection model that produces mild but sustained IOP increases and then studying the function of RGCs with a multielectrode array (MEA) (Cone et al., 2010; Sappington et al., 2010; Frankfort et al., 2013; Cowan et al., 2016a,b). With this approach, we have identified several RGC physiologic parameters that are extremely sensitive to even minimal IOP increases, suggesting a low threshold for IOP-related injury. In contradistinction, we have also identified RGC parameters that are unaffected by mild IOP elevation, suggesting a higher threshold for IOP-related injury. Finally, we uncover effects related to IOP magnitude by comparing these parameters at different IOP levels. The identification of distinct IOP-based functional thresholds for various RGC physiologic parameters has implications on both the study of IOP-related injury in mice and glaucoma staging and treatment in humans.

Materials and Methods

Experimental animals. Twelve-week-old C57BL/6J mice of both genders were used in this study. Mice were purchased from The Jackson Laboratory (stock #000664) and kept at Baylor College of Medicine facilities according to a standard 12 h light/dark cycle. All animal care and handling procedures were approved by the Institutional Animal Care and Use Committee of Baylor College of Medicine and were in accordance with the United States Public Health Service's policy on the humane care and use of laboratory animals.

IOP elevation and measurement. Animals that were to receive anterior chamber injection were anesthetized with a mixture of ketamine, xylazine, and acepromazine. Topical anesthesia with proparacaine 0.5% to the cornea was also given at the time of operation. To induce IOP elevation, 1.5 μl of polystyrene beads followed by 3.0 μl of sodium hyaluronate were injected into the anterior chambers ~15 d before MEA recording as described previously (Frankfort et al., 2013). For control animals, 1.5 μl of sterile saline was used instead of beads. IOP in uninjected eyes and in bead- and saline-injected eyes was measured with a TonoLab rebound tonometer (Icare Finland Oy) for rodents (Pease et al., 2011). IOP was measured within a tight window of 10:00 A.M. to 2:00 P.M. to minimize diurnal variation.

MEA recording. MEA procedures for mouse euthanasia, retina dissection, retina preparation and mounting, and fluidic maintenance have been described previously (Cowan et al., 2016a,b). Briefly, mice were dark-adapted for at least 90 min before the experiment. At the start of the experiment, deep anesthesia was initially induced by intraperitoneal injection of overdosed anesthetic mixture (ketamine 37.6 mg/ml, xylazine 1.9 mg/ml, acepromazine 0.37 mg/ml) and cervical dislocation was performed to euthanize the animal. Eyes were enucleated and quickly dissected in carboxygenated MEA buffer containing the following (in mM): NaCl 124, KCl 2.5, $CaCl_2$ 2, $MgCl_2$ 2, NaH_2PO_4 1.25, $NaHCO_3$ 26, glucose 22, pH titrated to 7.35, and bubbled with 95% O_2 and 5% CO_2 under infrared illumination using night vision scopes (B.E. Meyers). Whole-mount retinas were then separated from the eye and placed on the MEA face down so that inner retina was in direct contact to the electrodes. During the entire course of recording, the retina was perfused at 2 ml/min with prewarmed carboxygenated MEA buffer and was kept at 35.6°C by an on-stage heating element. All recordings were made from central regions of the retina. The MEA-60 (Multi Channel Systems) arrays provide 60 electrodes (10 μm in diameter and spaced 100 μm apart from each other) that allow us to collect action potentials from multiple RGCs simultaneously. Action potentials were sampled at 20 kHz and filtered with a 0.1 Hz high-pass hardware filter. Recording typically lasted 4–5 h for each retina. Spike isolation, sorting, and clustering were processed offline via standard procedures using customized MATLAB (The MathWorks) scripts (Cowan et al., 2016a; Sabharwal et al., 2016, 2017).

Light calibration. Visual stimuli were created with PsychToolbox in MATLAB. Images were presented on an OLED microdisplay (eMagin) and optically projected onto the RGCs through a beam splitter (Edmund Optics). The ambient light in the plane of array was measured as wavelength-specific irradiance in microwatts per square centimeter (S170C power sensor from ThorLabs and SpectraRad spectrometer from B&W Tek). The mean ambient light level was 3.07 $\log_{10}$ (R*/rod/s) for photopic conditions and -0.93 $\log_{10}$ (R*/rod/s) for scotopic conditions. Other than for the calculation of the spontaneous firing rate of RGCs (see below), only photopic results are presented here.

Criteria for model-fitting quality. RGCs in this study were presented with three types of visual stimulation: whole-field black/white screens (ON–OFF stimulation), binary white noise checkerboards, and whole-field contrast modulation at different levels. All RGCs were screened for two criteria to be included for further analysis: (1) adequate responses to whole-field black/white stimulation, represented by sufficient spike numbers and characteristic ON–OFF polarity and spiking transiencies (see below for details), and (2) presence of a well isolated RF represented by satisfactory spike-triggered averages (STA) fitting (r^2 based on the entire space–time map must be >0.3; see below for details). For more sophisticated analyses such as the Sum of Separable Subfilters (SoSS) model, r^2 fitting must also be >0.3.

Whole-field light stimulation and ON–OFF classification. Repeated alternative black/white screens (each lasting 4 s) were used to determine functional polarity (ON/OFF/ON–OFF) of the RGCs. An ON–OFF Index, defined in Equation 1, was calculated for each cell. ON cells had an ON–OFF index >0.7 and OFF cells had an ON–OFF index <-0.7. All other cells were classified as ON–OFF cells. Transient and sustained responses were qualitatively determined by manual selection, although we also calculated a transiency index (Eq. 2) to verify the classification.

$$\text{ON–OFF index} = (\text{response}_{ON} - \text{response}_{OFF})/(\text{response}_{ON} + \text{response}_{OFF}) \quad (1)$$

where response_{ON} and response_{OFF} refer to the number of spikes when the screen is white or black.

$$\text{transiency index} = \text{max peak response/mean maintained response} \quad (2)$$

where peak response is the number of spikes within a 0.5 s window after the onset of the stimulus and maintained response is number of spikes in the last 3 s of each stimulus.

White noise RF mapping and center and surround RFs. Methods used to map RFs were described previously (Cowan et al., 2016a; Sabharwal et al., 2016, 2017). Dynamic, random binary white noise checkerboards flickering at 15 Hz were presented to RGCs. Each element of the checkerboard was a 50 μm square and each checkerboard was composed of 32 × 32

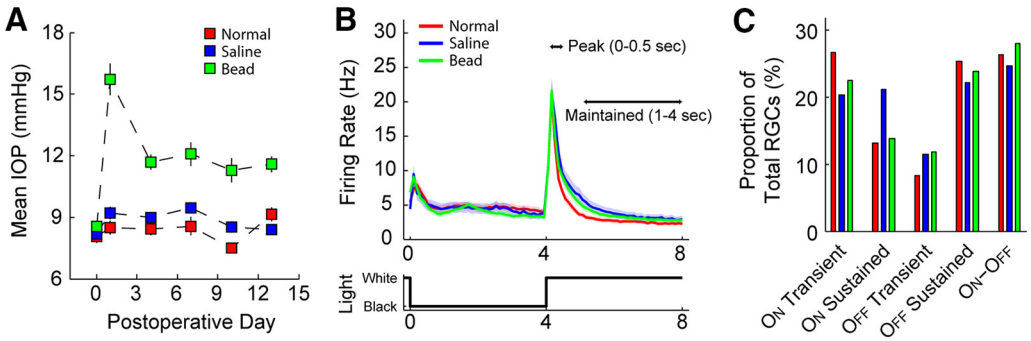

Figure 1. IOP and RGC classification. ***A***, Measured mean postoperative IOP was plotted for uninjected eyes (normal, red) and for eyes that were injected with saline (blue) or beads (green). Error bars represent ±1 SEM. ***B***, Mean firing rate of RGCs from normal eyes (red) and eyes injected with saline (blue) or beads (green) in response to whole-field binary stimulation. Shaded areas represent ±1 SEM. Peak response is defined as the number of spikes that occurred in first 0.5 s after the onset or offset of the stimulus; maintained response is defined as the number of spikes that occurred during 1–4 s after the onset or offset of the stimulus. The corresponding light level of the stimulation is illustrated at the bottom of the panel. ***C***, Proportion of five identified RGC subtypes (ON Transient, ON sustained, OFF Transient, OFF sustained, and ON–OFF) in normal eyes (red bars) and in eyes injected with saline (blue bars) or beads (green bars).

elements. The series of checkerboards (20,625) were created and presented through PsychToolbox (Brainard, 1997; Pelli, 1997). Spikes were collected and reverse correlated to the checkboard frames to calculate space–time STAs (Meister et al., 1994; Chichilnisky, 2001; Chichilnisky and Kalmar, 2002). STAs were fit to the product of a 2D spatial Gaussian and the impulse response of a temporal filter (Chichilnisky and Kalmar, 2002). The quality of STA fitting was assessed by r^2 as calculated from the complete space–time map of that cell. The size of a RF center was derived from major and minor axis of the Gaussian (Eq. 3). STA peak time for a RF was defined as the time it takes to reach the peak STA (either positive or negative) as follows:

$$\text{RF size} = \text{sqrt}(\sigma_x * \sigma_y) \quad (3)$$

where σ_x and σ_y represent 1-σ distance in major and minor axis of the Gaussian, respectively.

Temporal characteristics of center and surround RFs and their interactions were studied by first creating up to nine 1-σ annular zones for each RGC. A combined temporal trace within zones 1–3 or zones 4–9 was calculated and denoted as the center trace or surround trace. The time that a trace takes to reach its peak represents the temporal character of center or surround RF. A surround polarity index (SPI) was calculated to characterize the nature of the surround RF (Cowan et al., 2016a; Sabharwal et al., 2017); a negative SPI suggested opposite polarity between center and surround. As described previously (Cowan et al., 2016a; Sabharwal et al., 2016, 2017), the SoSS model interprets RFs as a sum of up to five independent subfilters, each having a unique spatial and temporal filter. SoSS modeling of the RFs was then used to estimate surround RF size (1-σ spatial extent of surround subfilter 1) and the temporal properties of the center RF in this study.

Spontaneous firing, interspike intervals (ISIs), variation of first spike time, and contrast sensitivity. Spontaneous firing of RGCs were recorded during scotopic sessions of the experiments that were at least 20 min before the beginning of photopic visual stimulation. Spikes were collected when the retina was not visually stimulated and was only exposed to ambient light.

The within-trial ISIs in the spike trains were obtained during binary black/white whole-field experiments. Because a substantial portion of our RGC population are transient cells, only the spikes occurring in the first 0.5 s after stimulation onset or offset were used for the ISI analysis. We then calculated and compared ISI variance across our RGCs. The same spike trains were used to compute trial-to-trial variation in the first spike time (measured as SD of first spike time in ms).

Whole-field stimulation at various contrast levels were used to investigate contrast responses of the RGCs. Eighteen Michelson contrasts ranging from 2.4% to 92% were presented in a random sequence and repeated twice. For each contrast, light intensity varied sinusoidally about a mean background (gray) at 2 Hz. Each stimulus was presented for 15 s with a preceding 5 s inter-stimulus interval. RGC firing was collected and fit with a Naka–Rushton function as follows:

$$R = R_{max} * (C^n/C^n + K^n) \quad (4)$$

where R and R_{max} are RGC response, C is the contrast, and K is the semisaturation contrast.

To quantify the lowest contrast to which RGCs can respond, we derived a "threshold contrast" for each RGC. After fitting with Equation 4, the lowest of three consecutive contrasts for which an RGC response reached the lower limit (mean − 1*SEM) of the normal responses was termed the "threshold contrast."

Experimental design and statistical analysis. Our MEA experiments used 53 C57BL/6J mice of both genders. Animals were randomly assigned to one of three treatment groups: microbead injection ($n = 24$, 14 males and 10 females), saline injection ($n = 18$, 10 males and 8 females), or no injection ($n = 11$, 6 males and 5 females). Saline injection was designed to control for potential effects from experimental procedures. The number of RGCs recorded from each animal varied.

All data are presented in the figures with means and SEMs. An ANOVA or Kruskal–Wallis test, depending on the normality of the data, was used to test the significance ($\alpha = 0.05$) of the changes among groups. Significant results warranted further comparisons between two particular groups. In such cases, p-values were adjusted for multiple comparisons using Fisher's LSD procedure. Two-factor linear regression model was used in more complicated comparisons involving more than one variable in experimental design (e.g., treatments and RGC subtypes) and are indicated as such in the Results.

Results

IOP elevation, RGC sampling, and classification

Eyes received an injection of beads or saline or no injection as described in the Materials and Methods. Bead injection induced mild and persistent IOP elevation over the 2 week study period (Fig. 1*A*). For bead-injected eyes, there was a transient spike of increased IOP from baseline the day after injection, followed by a stable return of IOP to 11.6 ± 3.64 mmHg (mean ± SD), which was statistically increased (one-way ANOVA, $p < 0.001$ for all postoperative time points). This dual-phase IOP change was not observed in the eyes that were injected with saline and saline-injected eyes showed no difference in IOP compared with normal (uninjected) eyes throughout the postoperative period (8.44 ± 1.49 mmHg for normal and 8.91 ± 1.95 for saline; Fig. 1*A*). RGCs for which RFs were identified were exposed to alternative black/white whole-field stimuli to characterize their ON/OFF responses. For 228 RGCs from uninjected eyes (red), 113 RGCs

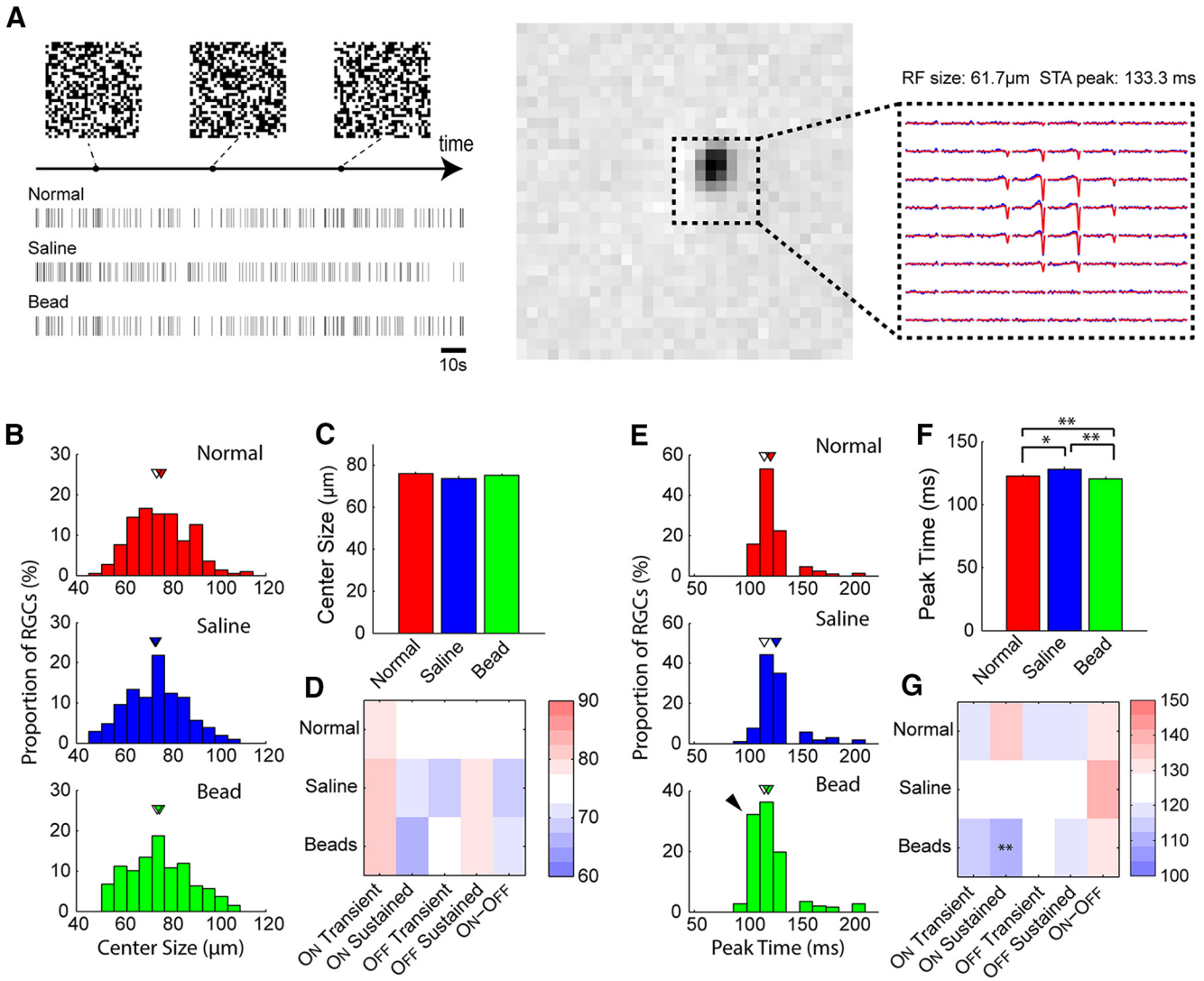

Figure 2. Size and STA peak time of center RF. ***A***, Identification of a cell's RF. Left, Example spike trains recorded during a trial of white noise for three representative cells: a normal cell (top), a cell from a saline-injected eye (middle), and a cell from a bead-injected eye (bottom). Stimulation was a series of 32 × 32 binary checkerboards (three example checkerboards are shown above the spike trains). Middle, STA of a cell under photopic light conditions revealing the location and spatial extension of the RF. Right, Mean STA (blue) and fit STA (red) traces for each checkerboard element within the dashed region of the STA. ***B–D***, Distributions (***B***), population means (***C***), and heat map (***D***) of center RF size in micrometers. ***E–G***, Distributions (***E***), population means (***F***), and heat map (***G***) of center RF STA peak time in milliseconds. ***B***, ***E***, Histograms showing distributions of the RGCs in normal eyes (red) and in eyes injected with saline (blue) or beads (green). Filled triangles are means and open triangles are medians. Arrowhead in ***E*** shows a significantly high proportion of RGCs having short STA peak time in bead-injected eyes. ***C***, ***F***, Population means. ***D***, ***G***, Heat map showing the difference in center RF size (***D***) or STA peak time (***G***) across major subtypes. In all panels, error bars indicate ±1 SEM. *$p < 0.05$, **$p < 0.01$.

from saline-injected eyes (blue) and 268 RGCs from bead-injected eyes (green), the mean firing rate was plotted as a function of the light level (Fig. 1*B*). Robust firing was elicited upon the onset and offset of the light and was maintained at a lower firing level during the rest of the stimulus. The mean firing rates from both saline and bead-injected eyes followed the same pattern as uninjected eyes and showed no significant difference at the peak (Kruskal–Wallis, $p = 0.117$) or during decay (Kruskal–Wallis, $p = 0.166$, as represented by the time constant).

The traces in Figure 1*B* are pooled responses of five functionally distinct RGC subtypes with different ON/OFF properties. Because these subtypes are so functionally distinct, it is possible that a sampling bias caused by bead or saline injection could affect our results. We therefore analyzed the proportions of each of the five major RGC subtypes in our three study groups (Fig. 1*C*). A χ^2 test suggested no significant differences among them ($p = 0.472$), ruling out that sampling bias confounded our findings.

Spatial and temporal characteristics of the center RF

We next calculated the size of the center RF. Comparable to data reported by others, the average center RF size was 75.9 ± 13.3 μm (mean ± SD) in uninjected eyes (Della Santina et al., 2013; Feng et al., 2013; Sabharwal et al., 2017). The center RF sizes for saline- and bead-injected eyes were 73.7 ± 12.5 and 75.1 ± 13.1 μm, respectively, which were not significantly altered from uninjected eyes (Kruskal–Wallis, $p = 0.509$; Fig. 2*B–D*). This suggests that neither surgical procedures nor IOP elevation caused apparent changes in center RF size on a population level. When looking at RGC subtypes (Fig. 2*D*), however, we found that center RF size varied across the five subtypes of the RGCs much more greatly in saline- and bead-injected eyes than in normal eyes (saline- and bead-injected eyes accounted for 47% and 43% of the total variation across subtypes, respectively). Nevertheless, there was no significant difference in center RF size for any RGC subtype.

We next assessed the temporal properties of RGC photopic responses in the center RF with the STA peak time and found

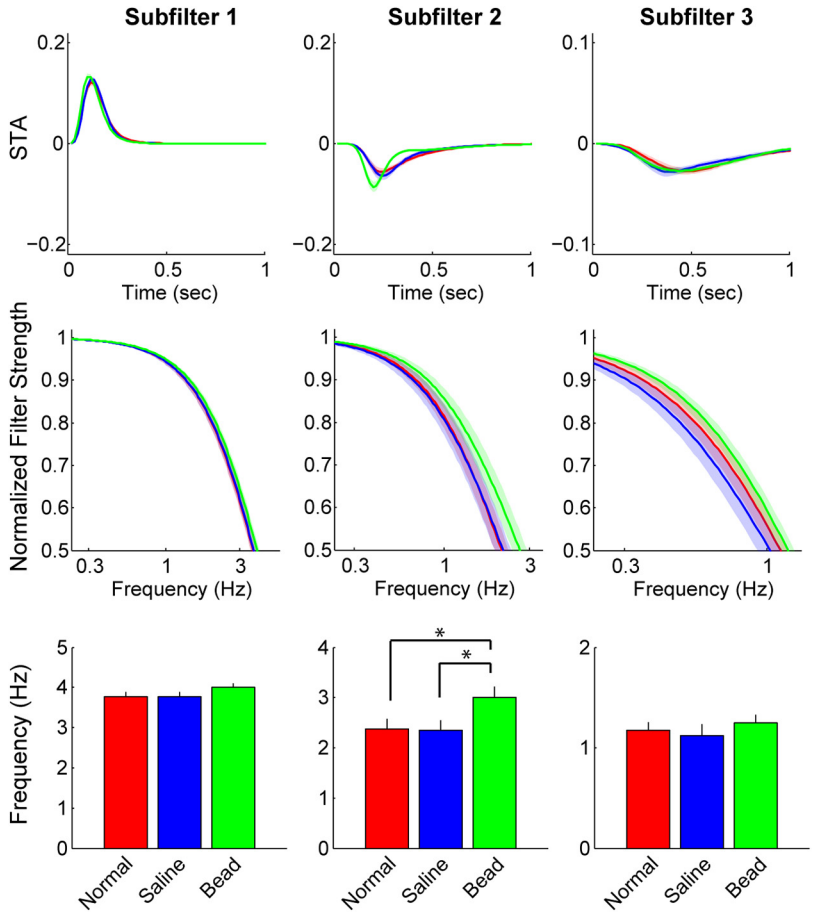

Figure 3. Subfilter temporal profiles of ON sustained RGCs. SoSS model-derived subfilters 1–3 in the time (top) and frequency (middle) domains. The corner frequency (bottom) of the center RF subfilters 1–3 are shown for ON sustained RGCs, a subset of our RGC population, from normal eyes (red) and eyes injected with saline (blue) or beads (green). Shaded areas and error bars indicate ±1 SEM. *$p < 0.05$.

significant differences among the three treatment groups (Kruskal–Wallis $p < 0.001$). Specifically, saline injection resulted in a slight but significant increase (i.e., delay) in STA peak time (Fig. 2*E*,*F*; adjusted $p = 0.012$), whereas bead injection caused a significantly shortened average STA peak time compared with either control (i.e., acceleration; adjusted $p = 0.004$ to normal and $p < 0.001$ to saline). When looking at peak time distributions instead of means, a sizeable proportion of the RGCs in IOP elevated eyes showed a shortened STA peak time (Fig. 2*E*, black arrowhead; Kolmogorov–Smirnov test, adjusted $p < 0.001$), implying that shortening of STA peak time in one or a few subgroups of the RGCs may offset the delay that we saw in saline-injected eyes. This was indeed the case because ON sustained RGCs had a shortened STA peak time and this change was highly significant when tested by a two-factor linear regression model (Fig. 2*G*; $p < 0.001$).

In light of this finding, we then investigated whether any subcomponents of the center STA changed significantly in ON sustained RGCs after IOP elevation. We used the SoSS model, a powerful tool to differentiate STA components, by separating it into up to five functionally distinctive subfilters that are closely related to different circuitry pathways (Cowan et al., 2016a; Sabharwal et al., 2016). We found that the average corner frequency of subfilter 2, a center antagonist STA component, was significantly increased (i.e., accelerated) in ON sustained cells after IOP elevation (Fig. 3; one-way ANOVA $p = 0.037$; adjusted $p = 0.029$ to normal and $p = 0.033$ to saline).

Spatial and temporal characteristics of the surround RF

We next assessed the spatial and temporal properties of the surround RF (Fig. 4*A*). Interestingly, a large proportion of RGCs lost their antagonistic surround following either saline or bead injection regardless of whether IOP was elevated (Fig. 4*B*; χ^2, both $p < 0.001$). Similarly, average peak time of the surround STA was significantly accelerated in both saline- and bead-injected eyes (Fig. 4*C*; Kruskal–Wallis $p = 0.001$; adjusted $p = 0.013$ to saline and $p < 0.001$ to bead). In a smaller group of RGCs in which RF surround size derived from the SoSS model was available, there was no difference in RF surround size among conditions (ANOVA, $p = 0.269$; Fig. 4*D*). To explore this unexpected finding in saline-injected eyes further, we looked at each of these properties according to RGC subtype (Fig. 4*E*–*G*). Interestingly, the proportion of RGCs having antagonistic surround was reduced by both saline and bead injection in ON transient cells (Fig. 4*E*, χ^2 test, $p = 0.007$ for saline and $p = 0.0029$ for beads), but only by bead injection for both OFF sustained and ON–OFF cells ($p = 0.0002$ for OFF-sustained and $p = 0.0001$ for ON–OFF cells). There was no subtype-specific reduction in average peak time of the surround STA or RF surround size (Fig. 4*F*,*G*, Kruskal–Wallis; *p*-values ranged between 0.0716 and 0.6375 for surround STA peak time of the RGC subtypes and between 0.1864 and 0.9938 for RF surround size). These subtype-specific findings imply a combination of a procedural effect from the injection technique and an additional effect of chronic IOP elevation.

Resting activity, spiking noise, and contrast sensitivity of RGCs

Changes in RF profiles represent alterations in the characteristic patterns used by RGCs to process upstream inputs, but do not tell much about the changes in RGC output. We investigated this by measuring RGC spontaneous firing, spiking noise (ISI variance and time to first spike), and response to various contrast levels. Spontaneous firing is an indicator of RGC excitability. IOP elevation caused a significant decrease in spontaneous firing of RGCs compared with saline-injected eyes (Fig. 5; Kruskal–Wallis $p = 0.016$, adjusted $p = 0.001$). Temporal precision of RGC spiking can be measured with both ISI variance and variation in time to first spike. IOP elevation caused an increase in average ISI variance of RGCs compared with saline-injected eyes (Fig. 5; Kruskal–Wallis $p = 0.019$, adjusted $p = 0.005$), but no significant change in variation in time to first spike (Fig. 5; $p = 0.532$). Together, these results suggest a potential reduction of signal fidelity from RGCs exposed to elevated IOP.

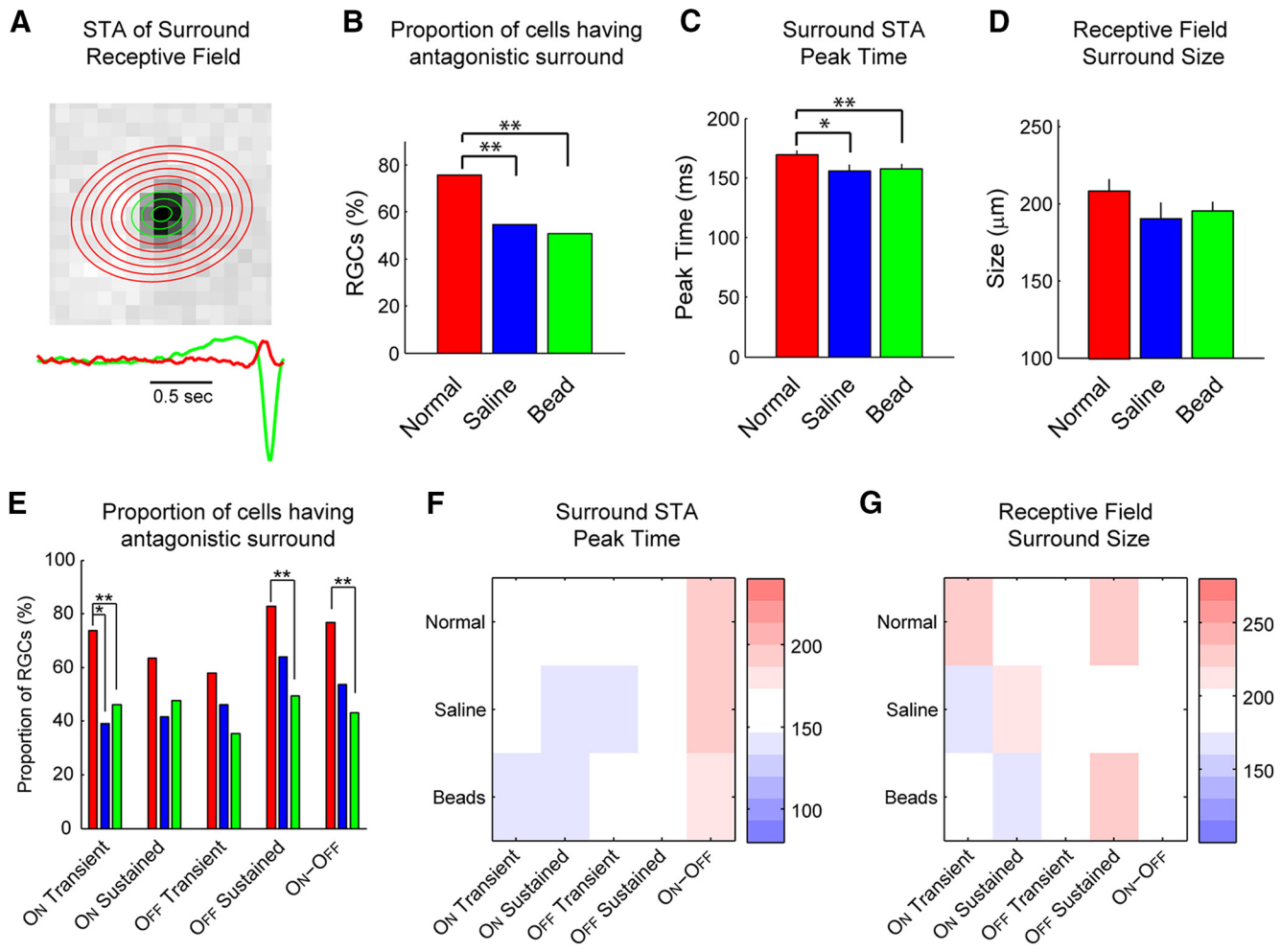

Figure 4. RF surround polarity. ***A***, Separation of center and surround RF. Temporal STA traces were pooled for center (green) and surround (red) annuli for a representative cell. ***B***, Proportion of the RGCs that demonstrated antagonistic surround RF (SPI < 0) from normal eyes (red) or eyes injected with saline (blue) or beads (green). ***C***, Mean STA peak time of the surround RF in RGCs. ***D***, Surround RF size. ***E–G***, Breakdowns of RGC proportions (***E***), surround STA peak time (***F***), and surround RF size for major subtypes (***G***). In all panels, error bars indicate ± 1 SEM. $^*p < 0.05$, $^{**}p < 0.01$.

Previously, we found that behavioral contrast sensitivity is affected even after short duration, mild IOP elevations in bead-injected eyes and therefore sought to explore this phenomenon at the cellular level (Fig. 6) (van der Heijden et al., 2016). Consistent with behavioral data, we found that when IOP was elevated, the ability of individual RGCs to respond to low contrast stimulation was significantly impaired, especially when contrast was below the threshold contrast of 8% (Fig. 6*C*; *t* tests, *p* values ranged between 0.0133 and 0.0451 for contrast levels ranging from 1% to 8%).

Effects of IOP elevation level on RGC function

Because our experimental glaucoma mouse model creates a range of magnitudes of IOP elevation, we used this attribute to extend our interpretation of resting activity, spiking noise, and contrast sensitivity according to IOP level. To do so, we first separated our bead-injected mice into two groups according to the magnitude of IOP elevation using a cutoff of 3 mmHg (Fig. 7*A*). We found that mild (<3 mmHg, 14 eyes, 160 RGCs) or moderate (>3 mmHg, 9 eyes, 108 RGCs) IOP elevation caused vastly different functional changes in terms of resting activity, spiking noise, and contrast sensitivity.

With this method, resting activity showed a clear IOP dependence and eyes exposed to moderate IOP elevation had a more profoundly decreased spontaneous firing rate compared with eyes exposed to mild IOP elevation (Fig. 7*B*; Kruskal–Wallis $p = 0.018$). Similarly, spiking noise also displayed a clear IOP dependence. Eyes exposed to mild IOP elevation showed an increase in ISI variance that was not statistically significant compared with either normal or saline-injected eyes and eyes exposed to moderate IOP elevation had a marked increase in ISI variance compared with normal eyes, saline-injected eyes, and eyes exposed to mild IOP elevation (Fig. 7*C*; Kruskal–Wallis $p < 0.001$). As above, we did not detect a difference in time to first spike (Kruskal–Wallis $p = 0.2498$), suggesting that only some aspects of spiking noise are affected by IOP. Finally, contrast sensitivity also changed dramatically according to IOP level. Although there was no significant reduction in RGC firing in eyes exposed to mild IOP elevation, in eyes exposed to moderate IOP elevation, there was a marked increase of the threshold contrast to 14% contrast (Fig. 7*D*; *t* tests, *p*-values ranged between 0.0024 and 0.0427 for contrast levels increased from 1% to 14%). This finding indicated that the impairment in contrast sensitivity is likely not manifested until a certain level of IOP elevation is reached.

To further illustrate the above observations, RGCs were binned into groups with a 2 mmHg step of IOP difference and functional metrics were plotted as a function of the mean IOP

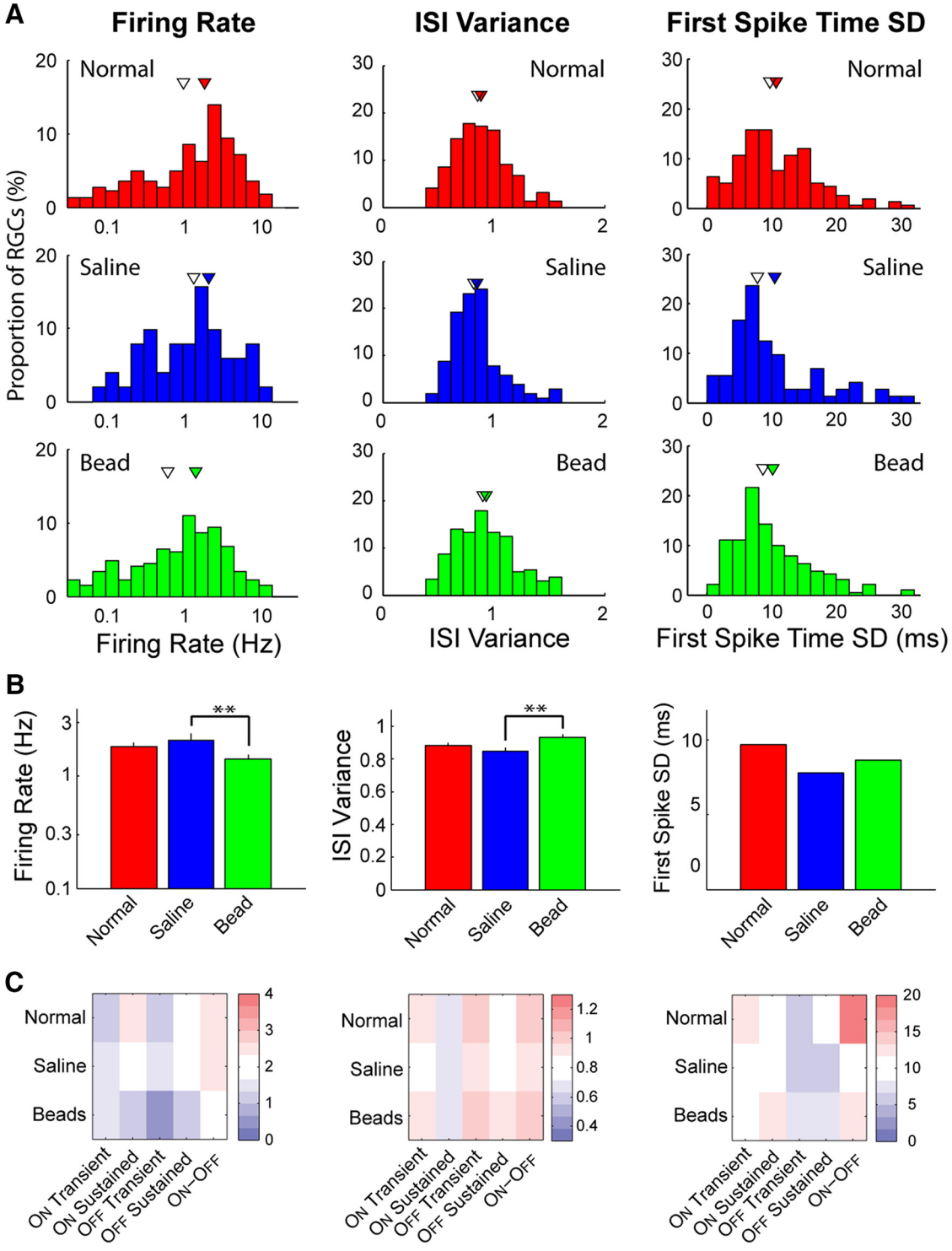

Figure 5. Spontaneous activity, ISI variance, and variation in first spike time. ***A–C***, Distributions (***A***), population means or medians (***B***), and heat maps (***C***) of spontaneous firing in Hertz (left), ISI variance (middle), and first spike time variation (first spike time SD, right) for normal eyes (red) and saline-injected (blue) or bead-injected (green) eyes. Filled triangles are means and open triangles are medians. Note that because variation in first spike time is much greater for ON–OFF cells than either ON or OFF cells, ON–OFF cells are included in the heat map but not the population analysis. In all panels, error bars indicate ±1 SEM. $^{**}p < 0.01$.

elevation (Fig. 7*E–G*). A negative correlation between spontaneous firing and IOP elevation was detected (Fig. 6*E*; $r^2 = 0.88$, $p = 0.063$) and a positive correlation was detected for ISI variance (Fig. 7*F*; $r^2 = 0.82$, $p = 0.094$). Threshold contrast did not have a clear linear relationship with IOP elevation, instead displaying a stair-like increase from the normal level when IOP elevation was >4 mmHg (Fig. 7*G*), consistent with the threshold effect seen in Figure 7*D*.

Discussion

Here, we report changes in RGC function after IOP elevation using the bead injection model. The average IOP increase and the

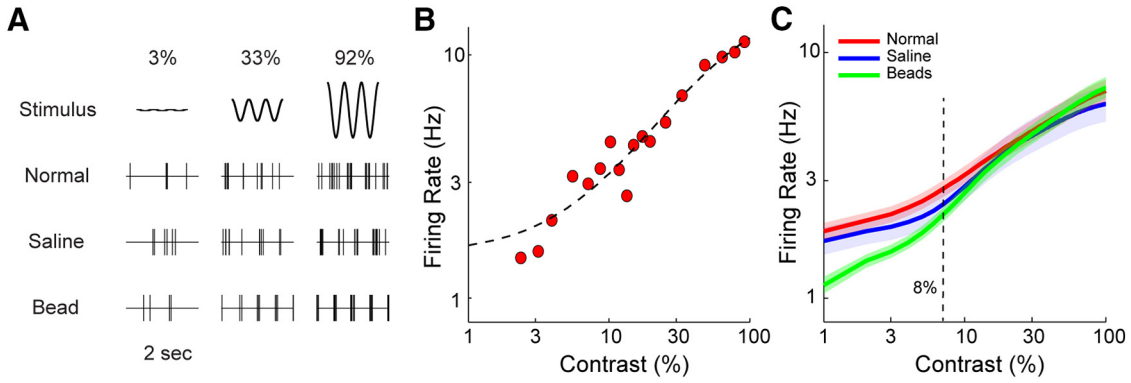

Figure 6. Contrast sensitivity. ***A***, Spike trains during low to high contrast are shown for three representative cells, one from each treatment group. ***B***, Firing rates (red circles) and fitting function (dashed line) of the first cell (normal) shown in ***A*** under different contrast conditions. ***C***, Firing rates of RGCs from normal eyes (red) and eyes injected with saline (blue) or beads (green) in response to different levels of whole-field contrast stimulation and fit with a Naka–Rushton function. Dashed vertical line indicates 8% contrast. Shaded areas indicate ±1 SEM.

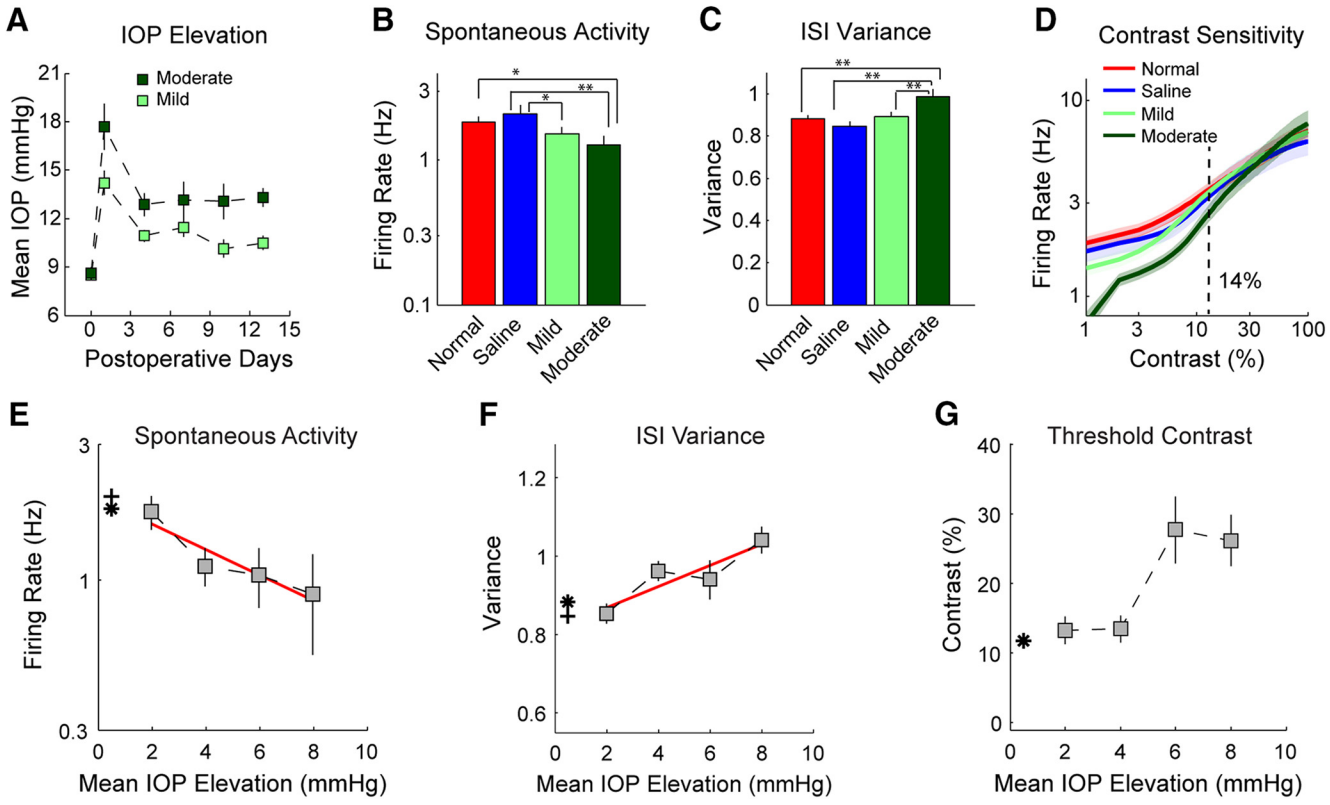

Figure 7. Effects of IOP elevation level on RGC function. ***A***, Replotting of mean IOP with bead-injected eyes stratified into mild (light green) and moderate (dark green) groups. ***B–D***, Spontaneous firing rate (***B***), ISI variance (***C***), and contrast sensitivity (***D***) were compared among RGCs from normal eyes (red), saline-injected eyes (blue), and bead-injected eyes (mild, light green; moderate, dark green). Dashed vertical line indicates 14% contrast. ***E–G***, RGC functions plotted against an IOP elevation gradient of 2 mmHg steps. Bold asterisk represents mean value of the RGCs from normal eyes. Bold plus sign (superimposed with asterisk in ***G***) represents mean value of the RGCs from saline-injected eyes. Solid red lines in ***E*** and ***F*** are regression lines. In all panels, error bars indicate ±1 SEM. $^{*}p < 0.05$, $^{**}p < 0.01$.

average absolute IOP level achieved in this 2 week study were considerably lower than their counterparts in other studies with similar designs (Della Santina et al., 2013; Feng et al., 2013; Ou et al., 2016; Sabharwal et al., 2017). This IOP difference creates an opportunity for the comparison of similar RGC physiological parameters between this mild IOP study and other higher IOP studies and to use these comparisons to establish IOP-dependent thresholds of dysfunction (Table 1).

Within this context, we found that RGC photopic RF center size was unchanged by mild IOP, whereas several other studies reported a decrease in RF center size (typically in OFF or ON–OFF cells) at higher IOPs (Della Santina et al., 2013; Feng et al., 2013; Ou et al., 2016; Sabharwal et al., 2017). This absence of RF center size reduction suggests that mild IOP elevation achieved in this study lies below the high IOP threshold needed to see this effect, even among susceptible RGC subtypes. Along the same lines, two of these studies assessed the properties of whole-field light responses and detected a range of abnormalities among multiple RGC subtypes (Della Santina et al., 2013; Sabharwal et al., 2017). We saw no such effect, which suggests that these high-contrast stimuli also have a high IOP threshold and the mild IOP elevation achieved in this study similarly lies below the critical threshold.

Table 1. Comparison of changes in measured RGC properties to existing literature

	IOP ↑ amount (mmHg)	IOP ↑ duration (days)	Photopic center RF size	Light evoked response	Photopic temporal	Spontaneous firing rate	Dendritic field*
This manuscript	~3	14–15	⇆	⇆	Acc	↓ (All)	NR
Risner	~4	14 or 28	NR	↑ at 14 d, ↓ at 28 d	NR	NR	↓ (variable among ON, OFF, ON-OFF)
Sabharwal	~7	13–16	↓ (All, ON-OFF)	↓ (OFF)	Acc	NR	NR
El-Danaf	~8	7	NR	NR	NR	NR	↓ (OFF sublamina)
Pang	~5–9	21–28 or 42–49	NR	↓ (ON, OFF)	NR	NR	NR
Della Santina	~10	15 or 30	↓ (OFF-T)	NR	NR	↓ (ON-S, OFF-S, OFF-T, ON-OFF)	↓ (OFF-T)
Feng	~15	~45	↓ (All)	NR	NR	NR	↓ (ON)
Ou	~15 at day 1, ~0 at day 7	7 or 14	↓ (OFF-T)	NR	NR	↓ (OFF-T)	↓ (OFF-S, OFF-T)

Variation in inter-spike interval, variation in time to first spike, and contrast sensitivity have not been reported elsewhere for animals with elevated IOP and are therefore not included.

* Dendritic field size was not reported in this manuscript but is included for completion.

↑ = Increased.

↓ = Decreased.

⇆ = No change.

NR = Not reported.

All = All RGCs.

ON-S = ON Sustained.

ON-T = ON Transient.

OFF-S = OFF Sustained.

OFF-T = OFF Transient.

Acc = Accelerated.

In contrast, we identified a prominent effect of mild IOP on the temporal properties of RGC photopic responses in the RF center. Specifically, temporal tuning was accelerated primarily in ON cells and most dramatically in ON sustained cells. This effect was most prominent in subfilter 2 of the SoSS model, which likely represents multisynaptic pathways of amacrine cells or narrow-field horizontal cells (Werblin et al., 1988; Cowan et al., 2016a). An effect on amacrine cells in experimental glaucoma is consistent with previous reports (Frankfort et al., 2013; Akopian et al., 2014, 2017; Pang et al., 2015; Sabharwal et al., 2017). We also detected a decreased RGC spontaneous firing rate, which has been identified in two other studies (Della Santina et al., 2013; Ou et al., 2016). These data suggest that both the temporal tuning of RGC photopic responses in the RF center and spontaneous firing rate have a low IOP threshold, one that is crossed by even the mild IOP elevations seen in this study.

How can we explain these distinct IOP thresholds? Photopic RF center size may be affected in a variety of ways, including by alteration of RGC dendritic structure and synapse dysfunction (Della Santina et al., 2013; Feng et al., 2013; El-Danaf and Huberman, 2015; Pang et al., 2015; Ou et al., 2016; Sabharwal et al., 2017; Risner et al., 2018). In contradistinction, RF photopic temporal properties are more likely driven by upstream cone and cone–rod circuits rather than dendritic or synaptic changes and acceleration may therefore represent the relative loss of a slower circuit, such as the rod BC–AIIAC synapse (Pang et al., 2004; Ke et al., 2014). This synapse has already been directly implicated in IOP-related injury and may therefore have a low IOP-related functional threshold (Pang et al., 2015; Sabharwal et al., 2017). The finding that ON cells were affected further supports this because intact gap junctions in AIIACs are required for most transmission of signal from rod BCs to ON RGCs and also mediate RGC injury due to increased IOP (Trexler et al., 2005; Pang et al., 2007; Akopian et al., 2014, 2017). Gap junctions are also important to allow for pooling of signal from the RF surround and we detected changes to antagonistic surround in mostly OFF and ON–OFF RGCs (Zhang and Wu, 2009). This could be explained by a decrease in surround signaling via AIIACs, which could in turn affect OFF RGCs via crossover pathways.

Other studies reporting phenotypes at higher IOPs have implicated OFF RGCs at both the functional and structural levels (Della Santina et al., 2013; El-Danaf and Huberman, 2015; Ou et al., 2016). Because OFF RGCs are regulated by AIIACs via glycinergic synapses, it is possible that this circuit has a high threshold to IOP-related injury, but shows a profound effect on RGC biology once it is crossed (Pourcho and Owczarzak, 1991; Pang et al., 2003). The absence of ON RGC effects in these studies may also imply that the ON RGC phenotypes seen here can be masked by higher IOPs, potentially via imbalances in upstream excitatory and inhibitory pathways. Another explanation is that ON RGCs have two critical thresholds, one that results in IOP phenotypes at low IOPs and another that extinguishes them at higher IOPs. Regardless, it is likely that distinct IOP-related and complex functional thresholds exist among retinal cell types and circuits.

Spontaneous activity, ISI variance, and contrast sensitivity were significantly altered by the mild IOPs achieved in this study, suggesting that each has a low-IOP threshold. Both RGC spontaneous activity and ISI variance reduced linearly with IOP even at the lowest IOP levels, further suggesting an IOP-dependent effect. However, we did not find abnormalities in first spike time variation, possibly because it was assessed with a light-evoked response in which the stimuli were not temporally rich (Berry et al., 1997; Keat et al., 2001; Uzzell and Chichilnisky, 2004; Murphy and Rieke, 2006). Regardless, additional work to reconcile these differences in RGC spiking fidelity and the impact of IOP level will be beneficial. One approach may be to determine whether IOP reduction from an increased level leads to a similar linear improvement in spontaneous activity and ISI variance, perhaps through the use of high-IOP models and IOP-lowering drops (John et al., 1998; Chen et al., 2011; Yang et al., 2012; van der Heijden et al., 2016).

Although RGC contrast sensitivity has been previously described at the cellular level, this is the first time it has been reported for experimental glaucoma (Zaghloul et al., 2003; Murphy

and Rieke, 2006; Tien et al., 2017). We found that RGC contrast sensitivity was reduced by increased IOP, but that this reduction was only apparent after IOP reached a specific level and then changed in a stepwise manner rather than linearly. This stepwise change suggests that the underlying mechanism is different than for spontaneous activity and ISI variance. Furthermore, the absence of response differences to high-contrast stimuli help to explain our finding that RGC peak firing rate to binary whole-field stimulation was normal. Indeed, it is possible that these high-contrast stimuli have a high IOP response threshold.

Abnormalities in behavioral contrast sensitivity have previously been described in animal models of glaucoma (Feng et al., 2013; van der Heijden et al., 2016) as well as in humans (Bierings et al., 2018a,b). In mice, these abnormalities could be prevented by IOP reduction (van der Heijden et al., 2016). A comprehensive understanding of the IOP threshold levels of various cellular processes (including contrast sensitivity) may thus allow for the development of clinical tests to probe the normality of these processes in humans, which would in turn result in improved diagnosis, staging, and risk stratification for patients with glaucoma.

Several properties of RGC photopic surround RFs were abnormal in RGCs exposed to either our IOP-elevating procedure or its procedural control. We found that saline-injected eyes had a decreased proportion of cells with antagonistic surround in the population and ON transient cells, with nonsignificant changes in the same direction among other RGC types, as well as an accelerated peak time across the population. These results may be explained by the acute IOP elevation due to volume effect that occurs at the very end of the injection in both experimental and control eyes. Consistent with this, other studies following acute IOP elevation have detected abnormalities in RGC function (Ou et al., 2016; van der Heijden et al., 2016). Chronic effects after an acute IOP event could in turn be caused by effects on either RGCs or upstream circuitry. With further analysis, it became clear that there was still some additional impact of chronic IOP elevation on the surround RF, namely the loss of antagonistic surround in OFF sustained and ON–OFF RGCs. This effect on OFF cells is more consistent with previous work, but comparison with other studies is limited by the fact that only one paper has reported the impact of IOP on the surround RF (Sabharwal et al., 2017). In any case, the use of two distinct controls allowed us to distinguish among likely IOP-related and procedural phenotypes and to determine that the injection procedure only affects a small subset of the RGC properties studied. Because many glaucoma models are induced and somewhat variable, this degree of scrutiny may be necessary to validate observations about the impact of IOP on RGC biology.

References

AGIS Investigators (2000) The advanced glaucoma intervention study (AGIS): 7. the relationship between control of intraocular pressure and visual field deterioration. Am J Ophthalmol 130:429–440.

Akopian A, Atlasz T, Pan F, Wong S, Zhang Y, Völgyi B, Paul DL, Bloomfield SA (2014) Gap junction-mediated death of retinal neurons is connexin and insult specific: a potential target for neuroprotection. J Neurosci 34:10582–10591.

Akopian A, Kumar S, Ramakrishnan H, Roy K, Viswanathan S, Bloomfield SA (2017) Targeting neuronal gap junctions in mouse retina offers neuroprotection in glaucoma. J Clin Invest 127:2647–2661.

Baden T, Berens P, Franke K, Román Rosón M, Bethge M, Euler T (2016) The functional diversity of retinal ganglion cells in the mouse. Nature 529:345–350.

Berry MJ, Warland DK, Meister M (1997) The structure and precision of retinal spike trains. Proc Natl Acad Sci U S A 94:5411–5416.

Bierings RAJM, de Boer MH, Jansonius NM (2018a) Visual performance as a function of luminance in glaucoma: the de Vries-Rose, Weber's, and Ferry-Porter's Law. Invest Ophthalmol Vis Sci 59:3416–3423.

Bierings RAJM, Kuiper M, van Berkel CM, Overkempe T, Jansonius NM (2018b) Foveal light and dark adaptation in patients with glaucoma and healthy subjects: a case-control study. PLoS One 13:e0193663.

Brainard DH (1997) The Psychophysics Toolbox. Spat Vis 10:433–436.

Chen H, Wei X, Cho KS, Chen G, Sappington R, Calkins DJ, Chen DF (2011) Optic neuropathy due to microbead-induced elevated intraocular pressure in the mouse. Invest Ophthalmol Vis Sci 52:36–44.

Chichilnisky EJ (2001) A simple white noise analysis of neuronal light responses. Network 12:199–213.

Chichilnisky EJ, Kalmar RS (2002) Functional asymmetries in ON and OFF ganglion cells of primate retina. J Neurosci 22:2737–2747.

Collaborative Normal-Tension Glaucoma Study Group (1998) The effectiveness of intraocular pressure reduction in the treatment of normal-tension glaucoma: collaborative normal-tension glaucoma study group. Am J Ophthalmol 126:498–505.

Cone FE, Gelman SE, Son JL, Pease ME, Quigley HA (2010) Differential susceptibility to experimental glaucoma among 3 mouse strains using bead and viscoelastic injection. Exp Eye Res 91:415–424.

Congdon N, O'Colmain B, Klaver CC, Klein R, Muñoz B, Friedman DS, Kempen J, Taylor HR, Mitchell P (2004) Causes and prevalence of visual impairment among adults in the united states. Arch Ophthalmol 122:477–485.

Cowan CS, Sabharwal J, Wu SM (2016a) Space–time codependence of retinal ganglion cells can be explained by novel and separable components of their receptive fields. Physiol Rep 4:e12952.

Cowan CS, Abd-El-Barr M, van der Heijden M, Lo EM, Paul D, Bramblett DE, Lem J, Simons DL, Wu SM (2016b) Connexin 36 and rod bipolar cell independent rod pathways drive retinal ganglion cells and optokinetic reflexes. Vision Res 119:99–109.

Della Santina L, Inman DM, Lupien CB, Horner PJ, Wong RO (2013) Differential progression of structural and functional alterations in distinct retinal ganglion cell types in a mouse model of glaucoma. J Neurosci 33:17444–17457.

El-Danaf RN, Huberman AD (2015) Characteristic patterns of dendritic remodeling in early-stage glaucoma: evidence from genetically identified retinal ganglion cell types. J Neurosci 35:2329–2343.

Feng L, Zhao Y, Yoshida M, Chen H, Yang JF, Kim TS, Cang J, Troy JB, Liu X (2013) Sustained ocular hypertension induces dendritic degeneration of mouse retinal ganglion cells that depends on cell type and location. Invest Ophthalmol Vis Sci 54:1106–1117.

Frankfort BJ, Khan AK, Tse DY, Chung I, Pang JJ, Yang Z, Gross RL, Wu SM (2013) Elevated intraocular pressure causes inner retinal dysfunction before cell loss in a mouse model of experimental glaucoma. Invest Ophthalmol Vis Sci 54:762–770.

Heijl A, Leske MC, Bengtsson B, Hyman L, Hussein M; Early Manifest Glaucoma Trial Group (2002) Reduction of intraocular pressure and glaucoma progression: results from the early manifest glaucoma trial. Arch Ophthalmol 120:1268–1279.

John SW, Smith RS, Savinova OV, Hawes NL, Chang B, Turnbull D, Davisson M, Roderick TH, Heckenlively JR (1998) Essential iris atrophy, pigment dispersion, and glaucoma in DBA/2J mice. Invest Ophthalmol Vis Sci 39:951–962.

Kass MA, Heuer DK, Higginbotham EJ, Johnson CA, Keltner JL, Miller JP, Parrish RK 2nd, Wilson MR, Gordon MO (2002) The ocular hypertension treatment study: a randomized trial determines that topical ocular hypotensive medication delays or prevents the onset of primary open-angle glaucoma. Arch Ophthalmol 120:701–713.

Ke JB, Wang YV, Borghuis BG, Cembrowski MS, Riecke H, Kath WL, Demb JB, Singer JH (2014) Adaptation to background light enables contrast coding at rod bipolar cell synapses. Neuron 81:388–401.

Keat J, Reinagel P, Reid RC, Meister M (2001) Predicting every spike: a model for the responses of visual neurons. Neuron 30:803–817.

Leske MC, Heijl A, Hussein M, Bengtsson B, Hyman L, Komaroff E; Early Manifest Glaucoma Trial Group (2003) Factors for glaucoma progression and the effect of treatment: the early manifest glaucoma trial. Arch Ophthalmol 121:48–56.

Meister M, Pine J, Baylor DA (1994) Multi-neuronal signals from the retina: acquisition and analysis. J Neurosci Methods 51:95–106.

Murphy GJ, Rieke F (2006) Network variability limits stimulus-evoked spike timing precision in retinal ganglion cells. Neuron 52:511–524.
Ou Y, Jo RE, Ullian EM, Wong RO, Della Santina L (2016) Selective vulnerability of specific retinal ganglion cell types and synapses after transient ocular hypertension. J Neurosci 36:9240–9252.
Pang JJ, Gao F, Wu SM (2003) Light-evoked excitatory and inhibitory synaptic inputs to ON and OFF alpha ganglion cells in the mouse retina. J Neurosci 23:6063–6073.
Pang JJ, Gao F, Wu SM (2004) Light-evoked current responses in rod bipolar cells, cone depolarizing bipolar cells and AII amacrine cells in dark-adapted mouse retina. J Physiol 558:897–912.
Pang JJ, Abd-El-Barr MM, Gao F, Bramblett DE, Paul DL, Wu SM (2007) Relative contributions of rod and cone bipolar cell inputs to AII amacrine cell light responses in the mouse retina. J Physiol 580:397–410.
Pang JJ, Frankfort BJ, Gross RL, Wu SM (2015) Elevated intraocular pressure decreases response sensitivity of inner retinal neurons in experimental glaucoma mice. Proc Natl Acad Sci U S A 112:2593–2598.
Pease ME, Cone FE, Gelman S, Son JL, Quigley HA (2011) Calibration of the TonoLab tonometer in mice with spontaneous or experimental glaucoma. Invest Ophthalmol Vis Sci 52:858–864.
Pelli DG (1997) The VideoToolbox software for visual psychophysics: transforming numbers into movies. Spat Vis 10:437–442.
Pourcho RG, Owczarzak MT (1991) Connectivity of glycine immunoreactive amacrine cells in the cat retina. J Comp Neurol 307:549–561.
Quigley HA, Broman AT (2006) The number of people with glaucoma worldwide in 2010 and 2020. Br J Ophthalmol 90:262–267.
Rheaume BA, Jereen A, Bolisetty M, Sajid MS, Yang Y, Renna K, Sun L, Robson P, Trakhtenberg EF (2018) Single cell transcriptome profiling of retinal ganglion cells identifies cellular subtypes. Nat Commun 9:2759.
Risner ML, Pasini S, Cooper ML, Lambert WS, Calkins DJ (2018) Axogenic mechanism enhances retinal ganglion cell excitability during early progression in glaucoma. Proc Natl Acad Sci U S A 115:E2393–E2402.
Sabharwal J, Seilheimer RL, Cowan CS, Wu SM (2016) The ON crossover circuitry shapes spatiotemporal profile in the center and surround of mouse OFF retinal ganglion cells. Front Neural Circuits 10:106.
Sabharwal J, Seilheimer RL, Tao X, Cowan CS, Frankfort BJ, Wu SM (2017) Elevated IOP alters the space–time profiles in the center and surround of both ON and OFF RGCs in mouse. Proc Natl Acad Sci U S A 114:8859–8864.
Sappington RM, Carlson BJ, Crish SD, Calkins DJ (2010) The microbead occlusion model: a paradigm for induced ocular hypertension in rats and mice. Invest Ophthalmol Vis Sci 51:207–216.
Tien NW, Soto F, Kerschensteiner D (2017) Homeostatic plasticity shapes cell-type-specific wiring in the retina. Neuron 94:656–665.e4.
Trexler EB, Li W, Massey SC (2005) Simultaneous contribution of two rod pathways to AII amacrine and cone bipolar cell light responses. J Neurophysiol 93:1476–1485.
Uzzell VJ, Chichilnisky EJ (2004) Precision of spike trains in primate retinal ganglion cells. J Neurophysiol 92:780–789.
van der Heijden ME, Shah P, Cowan CS, Yang Z, Wu SM, Frankfort BJ (2016) Effects of chronic and acute intraocular pressure elevation on scotopic and photopic contrast sensitivity in mice. Invest Ophthalmol Vis Sci 57:3077–3087.
Werblin F, Maguire G, Lukasiewicz P, Eliasof S, Wu SM (1988) Neural interactions mediating the detection of motion in the retina of the tiger salamander. Vis Neurosci 1:317–329.
Yang Q, Cho KS, Chen H, Yu D, Wang WH, Luo G, Pang IH, Guo W, Chen DF (2012) Microbead-induced ocular hypertensive mouse model for screening and testing of aqueous production suppressants for glaucoma. Invest Ophthalmol Vis Sci 53:3733–3741.
Zaghloul KA, Boahen K, Demb JB (2003) Different circuits for ON and OFF retinal ganglion cells cause different contrast sensitivities. J Neurosci 23:2645–2654.
Zhang AJ, Wu SM (2009) Receptive fields of retinal bipolar cells are mediated by heterogeneous synaptic circuitry. J Neurosci 29:789–797.